IEEE Access
Multidisciplinary ⋮ Rapid Review ⋮ Open Access Journal

Date of publication xxxx 00, 0000, date of current version xxxx 00, 0000.

Digital Object Identifier 10.1109/ACCESS.2024.Doi Number

3D Scanning of Hard-to-Reach Objects Using SfM-MVS Photogrammetry and a Low-Cost UAS

M.L. Gil-Docampo[1], Fellow, S. Peraleda-Vázquez[1], J. Ortiz Sanz[1], and Senior IEEE M.F. Cabanas
[1]Agroforestry Engineering Department, Universidad de Santiago de Compostela, 27002 Lugo SPAIN
[2]Electrical Engineering Department, Universidad de Oviedo, 33204 Gijón SPAIN

Corresponding author: M.L. Gil-Docampo (e-mail: m.gil@usc.es).

ABSTRACT SfM-MVS (Structure from Motion -Multi View Stereo) photogrammetry is a cost-effective and versatile technique used, among other applications, for the three-dimensional (3D) modelling of archaeological heritage sites and artistic objects. Traditional photogrammetry primarily derives the calibration parameters of the camera and the exterior orientation variables from ground control points (GCPs), obtained by means of a GPS, and tie points (TPs). The SfM-MVS approach simultaneously computes both the relative projection geometry and a set of sparse 3D points. However, when these techniques must be used with difficult-to-reach objects, the process is very complex and implies the use of expensive pieces of equipment. For these reasons, this study develops a new procedure to obtain 3D scale models using of a low-cost Unmanned Aerial System (UAS). To achieve good dimensional accuracy, a scaling tool has been designed which can be carried by the aircraft and deployed on the top of object. By means of this tool it is possible to determine the object actual size, scale the 3D model and then verify the operability and quality of the measurements obtained. The new method has been validated by comparing point clouds and distances. The results showed an error of less than 1 mm in almost 90% of the point cloud and a mean relative error of 1.49%. The procedure is therefore simple, effective and allows the use of SfM-MVS photogrammetry techniques indoors or outdoors on objects which due to their complex location, it is impossible to use scaling references and their reconstruction is only feasible with sophisticated and expensive technical means.

INDEX TERMS SfM-MVS photogrammetry, UAS, three-dimensional model, point clouds, objects inside building, difficult-to-reach objects. Low-Cost.

I. INTRODUCTION

UAS are increasingly present in different professional fields, ranging from precision agriculture, survey, search, and rescue (SAR), infrastructure inspection, to cultural heritage monitoring and cataloguing [1-3]. The incorporation of high-precision position sensors, obstacle detection and avoidance systems, and progressively sophisticated mission planners, has brought their use even closer to professionals and technicians by simplifying their operation and flight. The most commonly used aircrafts tend to belong to the professional segment of all manufacturers and especially to DJI™, which, in fact, monopolizes the world market. Despite their technical sophistication, their costs are high and not always affordable for end-users or researchers in general. For this reason, the number of research projects aimed at evaluating the ability of Low-Cost UAS to perform tasks such as facade inspection [7], monitoring of plant species, calculation of vegetation normalized indexes [8], obtaining thermographic digital terrain models [9], or generating point clouds and 3D models [10] has significantly increased. In others studies thermal or stereoscopic cameras have been installed in Low-Cost UAS to obtain 3D thermographic terrain models and accurate three-dimensional reconstruction of buildings [7,11]. By using stereoscopic cameras, [11], the behavior of the human vision is emulated, and the depth of the environment is estimated. With this procedure it is possible to perform stereo photogrammetry since the actual dimensions of the object are obtained from the distance between the cameras. The recording of overlapping images allows the use SfM-MVS techniques. These procedures are considered as automated photogrammetric methods of high resolution and low cost [14], which are also flexible and easy to apply

with a very fast learning curve [15]. The SfM-MVS is, in essence, based on the overlapping of the recorded images to find common points and thus generate a sparse three-dimensional point cloud, without the need for prior calibration [16]. To achieve this, it is necessary that the images present an adequate level of overlapping so that the processing software can identify homologous points between them [17]. Subsequently, MVS algorithms are applied to densify the sparse cloud from the already oriented images [18]. In addition, during image analysis, the software automatically determines the internal and external parameters of the camera [10].

Although different commercial products exist, all of them of high quality, one of the most widely used software packages in SfM-MVS is Agisoft Metashape™, largely due to its intuitive, user-friendly interface and automated workflow [15,19,20], which allows for easy generation of dense point clouds, 3D models, digital elevation models, and orthomosaics [21,22]. All these functions are also available in the software of other companies. PIX4D™ is another excellent tool, also used by the authors. Metashape™ has been preferred because of its greater ease of use and lower cost although the presented study can be carried out with open-source software as well. It is important to note that one of the main advantages of photogrammetry techniques is the absence of invasiveness; only by means of image processing it is possible to detect damage and/or defects in the reconstructed structure or object, and to maintain a continuous monitoring of the evolution of the entire affected area [23]. It is also possible to find abundant current research supporting the use of UAS inside buildings or facilities where the object to be study are not easily reachable: UAS positioning in an indoor space [24], real-time mapping [25], scanning of mine galleries [26], damage control after earthquakes [27] or industrial inspection [28].

The field of application of UAS as a work tool is thus expanded, and their use is facilitated, in legal terms, since, while flying inside an enclosed area or installation, the aircrafts are not subject to the regulations of the European Union Aviation Safety Agency (EASA) or the European legislation applied in Spain by the State Safety Agency (AESA), apart from the fact that adequate safety measures must be maintained.

It is important to point out that in existing applications for flight inside buildings, it is necessary to know the flight map of the building and provide the environment with sensors and beacons, or to use expensive and sophisticated UAS capable of crashing into walls, [26]. To the best of the authors' knowledge, the 3D reconstruction of difficult-to-reach-objects, even inside any kind building by simply transporting a scaling tool, to be placed on top of the object - where to do so by “conventional means”- would involve the use of scaffolding or complex structures, has never been tested. Moreover, existing procedures using total stations or high-resolution scanners, although undoubtedly very accurate, also involve expensive and relatively complex instrumentation. The proposed method, however, is within the reach of any researcher and is extremely simple as will be shown later. The accuracy obtained with it is good, and it democratizes, especially in the field of historical heritage conservation, the obtaining of 3D models with a more than reasonable quality and a very low cost.

II. MATERIALS AND METHODS

This section will define the objectives of the study, the material means; test specimen, UAS, and camera used. In later sections, the methodology and the results will be shown and validated.

A. OBJECTIVES

The objective of this study is to develop a SfM-MVS method to obtain three-dimensional scaled models of objects with no dimensional reference, or that to approach them require the installation of complex infrastructure such as scaffolding, ladders or support structures. The installation of these additional means may condition and delay the work, especially if the object to be modelled is of significant heritage value and is found in sites which, for this same reason, are open to the public. In order to solve or reduce the above problems and minimize costs, a low-cost UAS will be used, and a transportable system will be designed to find out the actual dimensions of the object and scale the model with millimetric precision. The operability of the method will be demonstrated, and the quality of the obtained measurements will be experimentally evaluated. As will be shown in the conclusions, this new procedure opens up multiple possibilities not currently considered, to the best of the authors' knowledge, to carry out studies in most of the fields mentioned in the introduction.

B. TEST SPECIMEN, UAS, AND DIGITAL SINGLE LENS (DSLR) CAMERA

The object selected for the three-dimensional reconstruction was a granite rock with an irregular geometry. This material has been chosen because of its historical use in construction in Spain [29]. In fact, it is the most common material in the cultural heritage of the northwest of the Iberian Peninsula [30]. Galicia has a large number of granite quarries and is one of the three major producing areas of this materia [31,32]. For the above reasons, the interest in using a granite rock as a test specimen is evident if the work is focused on the conservation of architectural heritage. In any case, using any other material whose surface texture is suitable for the application of SfM-MVS techniques would be equally valid and would not alter the obtained results. The rest of the material means is very simple and cheap: a low-cost UAS, whose specifications will be presented later, a digital caliper for manual measurements, and a device manufactured in plastic, by 3D printing, that is transported by the aircraft. To hold the scaling tool to the UAS, carbon fiber rods of different

lengths, sections, and rigidity, depending on the inaccessibility of the object, and a simple anchoring system attached to fuselage surface will be used. The work method is as simple as placing the scaling tool on the unreachable object and obtaining a set of overlapping photographs, flying around it, from all possible angles as an insect would do. For the design of the anchoring system and the scaling tool, a large number of tests were made assessing the flight stability of the UAS, its maximum payload, and obtaining different anchoring systems and scaling tools of different materials, so that the cost and the complexity of handling as well as the possibility of placing the scaling tool even in really adverse accessibility conditions were possible. During the laboratory tests, a scaling tool 3D printed in Acrylonitrile Styrene Acrylate (ASA) was used because it is the lightest plastic for 3D printing and the targets used were cut in vinyl with a cutting plotter. This option was chosen because of the durability of the tool, which is materially impossible to break or degrade. In later sections it will be shown that it is not necessary to use a 3D printer; different scaling tools, even made with printed paper from a laser or ink injection conventional printer, will be presented. The rods for transport will also be studied and it will be shown how taking advantage of their flexibility, and length, and varying their section, not only reduces even more the cost and weight, but it also allows to obtain the configuration of the arrangement that is more comfortable and efficient for the flight. Tests were also carried out by deactivating the aircraft's lower vision sensors, which facilitate a stable positioning of the aircraft when hovering, since their operating range, depending on the lighting conditions, does not exceed 30 m and the method is aimed to be used in the most adverse conditions. For this purpose, the two cameras oriented to the floor were covered with black adhesive tape and it was possible to check how deploying the tool onto the test specimen, in a completely manual flight, presents no problems, especially if a scaling tool and a very low weight transport system are selected. A flight test without position sensors can be watched in [34].

To carry out laboratory research, a rope system was built to lift the test specimen as can be seen in Figure 1. For the selection of the UAS, the one with the smallest price and dimensions was chosen; a DJI Mavic Mini 1™. Its dimensions are 245 x 289 x 55 mm unfolded with propellers, and its weight is 249 g. Due to its small size, it is easily maneuverable indoors, and can fly in narrow or difficult areas without colliding, as it has an obstacle detection system. It is the lowest cost model offered by the company, priced at €349, which includes 3 additional batteries and propeller guards, useful for indoor flying, but which were not necessary to install during the study.

The use of the UAS transmitter, combined with a mobile device, allows First Person View (FPV) flight, and the camera in nadir position provides a high-resolution real time image which makes it even easier to position the scaling system on the object. Table 1 shows the specifications of the aircraft camera and Table 3 the properties of its stabilizer. Figure 2 is a picture of the drone and all accessories and Figure 3, taken from the manufacturer's manual of the UAS, shows all its sensors.

FIGURE 1. Test specimen lifted by the rope system.

To assess the quality of the results obtained with the drone, a professional Canon EOS 2000D™ DSLR camera was used. Its APS-C™, Complementary Metal Oxide Semiconductor (CMOS) sensor, whose size is 22.3 x 14.9 mm, presents a resolution of 24 megapixels (6000 x 4000 pixels), which produces a pixel size of 3.72 x 3.73 µm. The lens installed was a Canon EF-S™ 18-55 mm f/3.5-5.6, carefully adjusted at 18 mm. The results were evaluated by manually taking pictures with the camera at the same average distance, processing them, and generating a second dense point cloud, which was compared with the dense point cloud obtained from the images taken by the drone camera.

Since a variable focal length lens has been used and the validation implies to check the accuracy of results, this part of the study will be shown in detail in the next section.

The process of verifying the results and scaling the model involves taking a significant number of direct measurements on the surface of the test specimen. To do this, in a simple and reasonably precise way, a Mitutoyo Absolute Digimatic™ 500-161-20 digital caliper was used, which measures in a range of 0 to 150 mm and allows measurements to be taken with a resolution of 0.01 mm. It is important to bear in mind that, in addition to the resolution of the gauge, there is a random error involved in manual measurement. Furthermore, as will be discussed later, even by selecting singular points of the rock, it is materially impossible to take a perfect measurement, especially considering its granular nature.

TABLE 1: DJI Mavic Mini 1™ camera specifications

CAMERA	
SENSOR	1/2.3" — CMOS
EFFECTIVE PIXELS	12 Mpx
RESOLUTION	4:3 — 4000 x 3000 16:9 — 4000 x 2200

FIELD OF VIEW (FOV)	83º
FOCAL DISTANCE	24 mm (35 mm equivalent)
APERTURE	f/2.8
ISO RANGE AUTOMATIC	100 — 1600
ISO RANGE MANUAL	100 — 3200

C. SfM-VMS SOFTWARE

For image processing and three-dimensional reconstruction both of the set of photographs taken with the DSLR camera and those recorded by the UAS camera, as stated in previous sections, and for the reasons mentioned above, Metashape Professional™ v1.6.5 as used as this was the version available at the time of the study.

TABLE 3: DJI Mavic Mini 1™ stabilizer specifications

STABILIZER	
MECHANICAL RANGE TILT	110º TO 35º
ROTATION	-35º TO 35º
CONTROLLABE RANGE TILT	-90º TO 0º (DEFAULT) (EXTENDED)
SWIVEL	-20º TO 20º
ANGULAR VIBRATION	±0.01º
STABILIZATION	3 AXES
MAX. CONTROL SPEED	TILT: 120º/s
TYPE OF CONTROL	AUTOMATIC/MANUAL

FIGURE 2. DJI™ Mavic Mini 1 combo with all its accessories.

FIGURE 3. DJI™ Mavic Mini 1 optical flow positioning system.

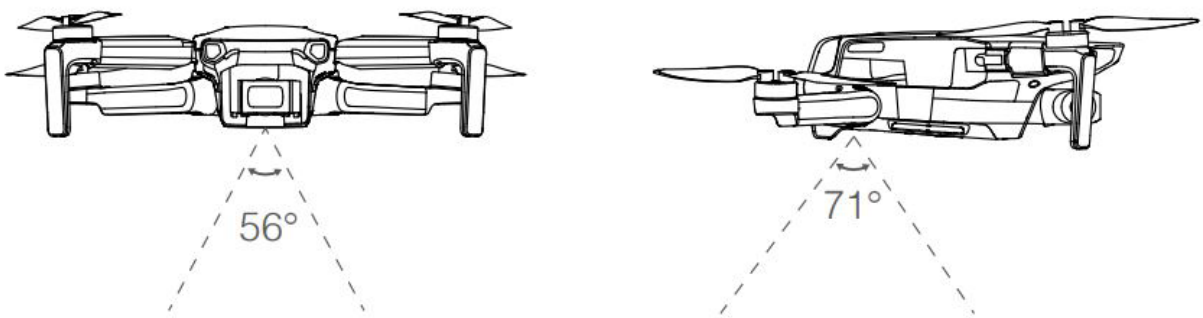

As stated above, to assess the quality of the results obtained with the drone, a Canon EOS 2000D™ DSLR camera was used. Its APS-C™, Complementary Metal Oxide Semiconductor (CMOS) sensor, whose size is 22.3 x 14.9 mm with a Crop Factor of 1.6, presents a resolution of 24 megapixels (6000 x 4000 pixels), which produces a pixel size of 3.72 x 3.73 µm. The lens installed was a Canon EF-S™ 18-55 mm f/3.5-5.6 with the focal length carefully adjusted and mechanical fixed to 18 mm. Although in the application of Sfm-MVS techniques the use of variable focal length lenses, although valid, is not the optimal choice, the aforementioned lens was used to reach a comparison of the results where the properties of the two cameras were as similar as possible, except for the resolution, where the DSLR camera was taken

as the reference. The results were evaluated by manually taking pictures processing them, and generating the dense point cloud, which was compared with the dense point cloud obtained from the images taken by the drone camera. The average distances at which photographs were taken with the UAS and the DSLR camera were 0.75 m and 0.42 m respectively. Table 2 presents the specifications of the lenses, sensors, and resolutions of the DSLR camera and that of the Mavic mini I™. It can be observed how the DSLR camera is an accurate reference as its Ground Sampling Distance (GSD), not calculated in this case from the ground but to the distance from the object, is 0.087 mm/px whereas with the Mavic Mini's camera, the value obtained is 0.27 mm/px, i.e. the DSLR camera resolution is 3.1 times higher than that of the UAS. If with slightly more than three times the resolution of the manually taken photographs both point clouds show residual differences, the accuracy and validity of the results are proven.

TABLE 4: Comparison between DSLR and Mavic mini I™ cameras

CAMERA	SENSOR	NUMBER OF Px	Px DIMENSIONS	RESOLUTION	FOCAL DISTANCE	35 mm EQUIVALENT FOCAL DISTANCE	GSD DISTANCE (0.42-0.75 m)
CANON EOS 2000 EF	22.3x14.9 mm	6000x4000	0.0037x0.0037 mm	24 Mpx	18 mm	29.1	0.0087 mm/px
MAVIC MINI I	1/2,3" - 6.17x4.55 mm	4000x3000	0.0015x0.0015 mm	12 Mpx	4,25 mm	24.0	0.27 mm/px

For the comparison of the dense point clouds CloudCompare version 2.11.3 was used. CloudCompare is public domain software that allows to process point clouds, triangular meshes and compare them both homologous; (point cloud vs. point cloud) or mixed; (point cloud vs. triangular mesh). The software also includes several plug-ins with additional functions.

D. SCALING TOOL

For image processing and three-dimensional reconstruction both of the set of photographs taken with the DSLR camera and those recorded by the UAS camera, as stated in previous sections, and for the reasons mentioned above, Metashape™ was used.

To achieve the scaling and orientation of the model, a device that could be carried by the UAS and placed on top of the test specimen was designed. This tool must be easily picked up by the aircraft in the same way as it is released at the study site. The first step before starting its geometric design and construction was to determine the maximum takeoff weight (MTOW) that a Mavic Mini I™ could carry without compromising its flight and maneuverability. Multiple tests were carried out and it was concluded that the limit was 137 grams, approximately half its weight. This result was predictable as the thrust-to-weight ratio for multi-rotor aircrafts, and in particular DJI™ products, is usually greater than 2.

Once the MTOW was found out, an easy to build three-dimensional structure was selected and manufactured with a weight much lower than the maximum. A triangular prism was chosen, with three support legs and dimensions of 120 mm on each side and 70 mm in height. It was manufactured by 3D printing in Acrylonitrile Styrene Acrylate (ASA), an amorphous synthetic thermoplastic that is the lightest and most durable of all available plastics. 54 targets were cut out of black vinyl with a cutting plotter and pasted on the prism. The design of the targets has been included Appendix A where it can be seen how they have been built with concentric circle sectors.

The 3D printing was done with a filling factor of a 10% to reduce the weight. A 1 mm diameter carbon rod was installed in the shape of a circle, with a relatively large diameter, to facilitate its release and collection at the top of the prism. The final weight of the tool was 32 gr. Plastic was chosen to achieve a solid and durable scaling tool that would allow multiple experimental tests to be carried out without degradation. Figure 4 shows the complete set of targets (included in the Appendix A), the prism and the carbon fiber ring for release and transport using during the study. Figure 5 is a photograph of the system installed on the UAS to transport the prism.

For the development of the method, a large number of targets were used, which can be placed in any position on the prism and in any order. However, for scaling, it is not necessary to use such a large number of targets, since knowing the distance between two targets is sufficient. Figures 6 and 7 show other tools made of cardboard and paper, which are much lighter and have a smaller number of targets. These figures show the prism without legs, which is the design for a flat surface. Since the aim of this study is to be able to produce models of objects with limited accessibility and complex geometries, the possibility of not having flat surfaces for their placement was considered in the design of the scaling tool.

For objects with irregular geometry (e.g. a lamp) it is sufficient to add 3 carbon rods of 1 mm and let the scaling device fall at any point, as the position of the prism does not influence the result.

The anchorage system may be attached to either the upper or lower fuselage of the aircraft. The most convenient option is to do it on the upper part, in those cases where it is possible to use the optical flow sensor to facilitate flight, since it is

difficult to do it on the lower part without interfering with the vision of the positioning cameras. In the event that the object is at an altitude where optical flux cameras the cameras no longer correct the position, it is possible to fix it at the top or at the bottom indistinctly. In the event that the object is at an altitude where the cameras no longer correct the position of the UAS, it is possible to fix it at the top or at the bottom indistinctly. It is also possible to use hooks and rods of different lengths (Figure 8) by reducing their cross-section and using the lower weight prisms shown in Figures 6 and 7.

To give the transport system even more flexibility, a small ASA connector allows the length of the rod to be extended if necessary. It is clear that the lengthening of the rod is limited by the torque exerted on the fuselage, and that a curved bending of the rod will occur, especially when the length is extended. One might think that the downward curvature of the rod creates a problem, however, for objects in very high positions, it facilitates the deployment of the scaling tool, which "hangs" in a lower position than the UAS and is visible through the FPV system. In fact, the position obtained with the designed system allows the camera to be manually rotated to nadir or intermediate position, in such a way that the image of the FPV system allows the prism to be positioned using all the different transport systems even without a clear direct view. It should be noted that the test specimen was installed in a laboratory, since the development of the method, which involved a long experimental process, did not allow the use of reference objects belonging to a building that could be easily accessed and where all the necessary means and tools for the research could be found. The aim of this paper is therefore to demonstrate the feasibility of the new method, to prove its accuracy, and to provide other researchers with the necessary tools to reproduce it, considering its application, as can be seen in the audiovisual material [34], in the most adverse conditions. Section E will show an image of an actual case that will be worked on by obtaining architectural models in a study in the field of cultural heritage conservation. The image will show that the implementation of the new method is field-study cases is simpler than the one presented in this article.

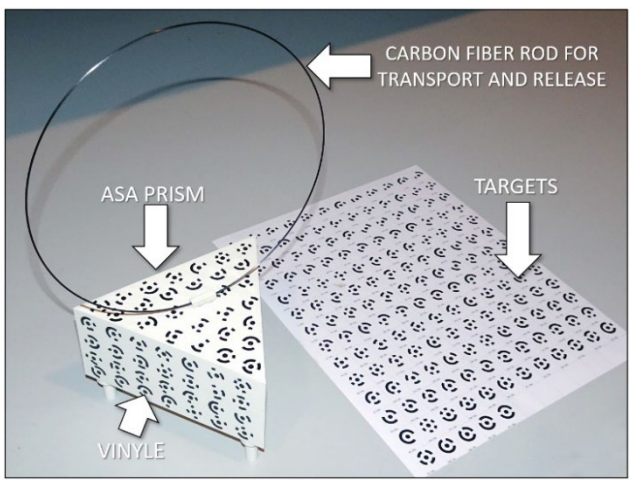

FIGURE 4. Targets and scaling tool used during the study.

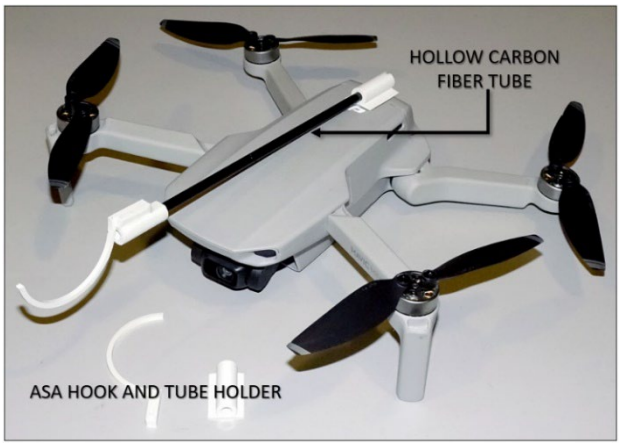

FIGURE 5. UAS with the transport and release hook installed.

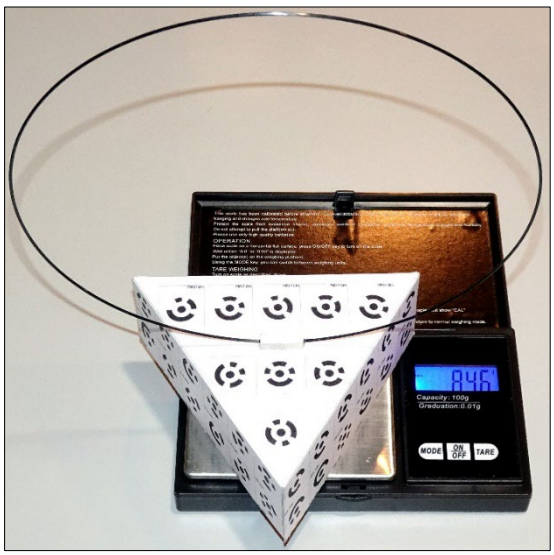

FIGURE 6. Option A: scaling tool built with cardboard, 8.46gr.

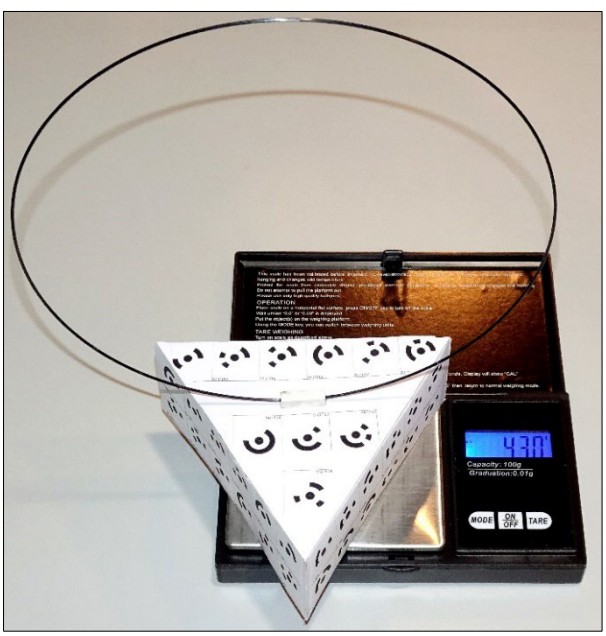

FIGURE 7. Option B: scaling tool built with paper, 4.3 gr.

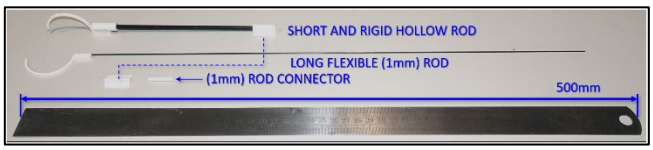

FIGURE 8. **Different options of rod: multiple possibilities of transport.**

III. RESULTS AND DISCUSSION

The methodology used in the study is represented by the flow chart in Figure 9. The first step consists of the installation of the scaling tool on the top of the test specimen. Recording the photographs is done both with the scaling device placed on top of the test specimen and without it. In the second case, the photos that complete the model are taken in the area occupied by the prism; before placing the prism, during its removal or once it has been removed. Figure 10 shows the UAS in flight at maximum speed transporting the scaling tool.

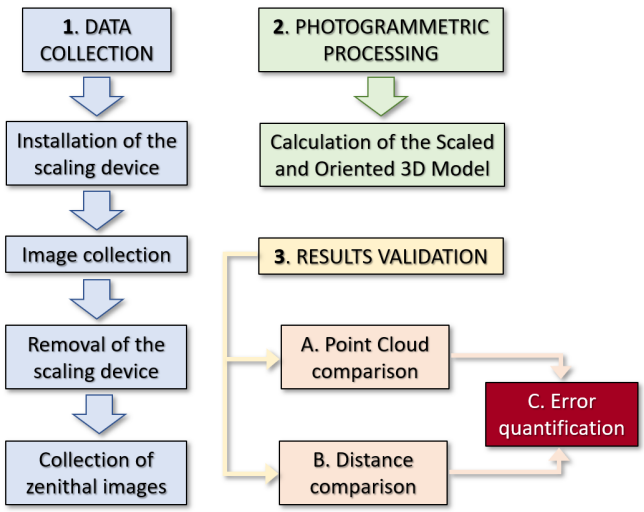

FIGURE 9. **Flowchart with the methodology of the whole study**

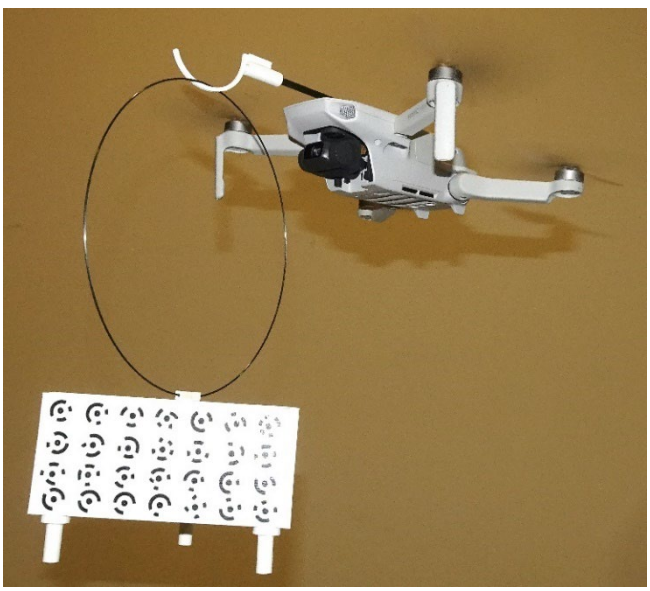

FIGURE 10. **UAS transporting the scaling tool at maximum flight speed: only a slight swaying of the load is perceptible.**

Once the prism was in place, a large set of overlapping photos were taken around the test specimen with both the UAS and the DSLR camera. When this part of the process was completed, the prism was removed, again by means of the UAS, and the photographing was repeated from nadir position. In total, 261 photographs were taken with the UAS and 199 with the camera. The average shooting distance was 751 mm and 421 mm respectively. Image processing is performed following the standard workflow implemented in Metashape™. First, the images are uploaded and reviewed. In the case of the images acquired with the UAS, a prior selection was made to use only those with the highest sharpness and best overlapping, for which the number of photographs was reduced to 143. The next step is the creation of masks on the images, delimiting the area of interest. This step is especially important in the case of pictures taken with the UAS camera. Its 83º Field of View (FOV), together with the distance between the camera's CMOS sensor and the test specimen, causes a certain level of background noise to appear. The introduction of masks eliminates excess pixels in the background while significantly decreases processing time. Once the images are properly prepared, the photogrammetric processing follows the flowchart in Figure 11.

FIGURE 11. **Photogrammetric processing flowchart.**

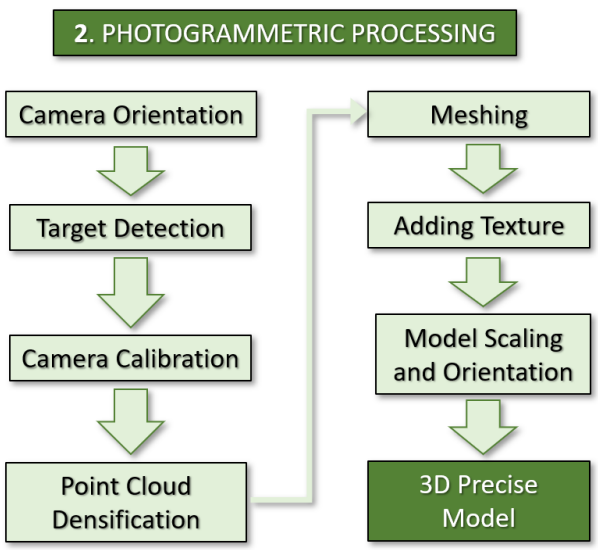

As soon as the sparse point cloud is created, the “Detect Targets Tool” is used, which automatically identifies the coded targets. The images are checked to ensure that the markers are correctly numbered and positioned. Of the 54 targets, the software successfully detected 51. The targets act as tie points between the images with an accuracy of less than one pixel. Next, the camera calibration is performed using the “Optimize Camera Orientation Tool”, within which the focal parameters (f), coordinates of the main point of the photograph (cx, cy) and radial and tangential distortion coefficients (k1, k2, k3, p1, p2) are adjusted. Subsequently, the dense point cloud is generated, in high quality, and with a slight filtering,

and then the mesh is built to produce the triangulation of the model, using the depth maps as source data, selecting high quality too. Finally, a realistic texture is formed from the images, thus obtaining the final appearance of the model. The scaling and dimensional adjustment procedure will be shown later.

A. 3D MODEL

Table 2 shows the results obtained in the processing of the images collected by the UAS camera and the properties of the 3D model.

TABLE 5: 3D model data and processing time

Sparse Point Cloud	63,988 points
Dense Point Cloud	1,615,352 points
3D Model	257,891 points
Processing Time	42 minutes and 46 seconds

B. POINT CLOUD ANALYSIS AND VALIDATION

For the comparison of the dense point clouds generated in Metashape™, Cloud-Compare was used. First, they were exported in LAZ format and loaded into Cloud-Compare after removing excess points. Then, the Multiscale Model to Model Cloud Comparison (M3C2) method was applied. This mathematical procedure computes the local distance between two different point clouds along the normal surface direction which tracks 3D variations in surface orientation. The point cloud generated from the DSLR camera images was taken as a reference, leaving the rest of the program parameters at their default settings.

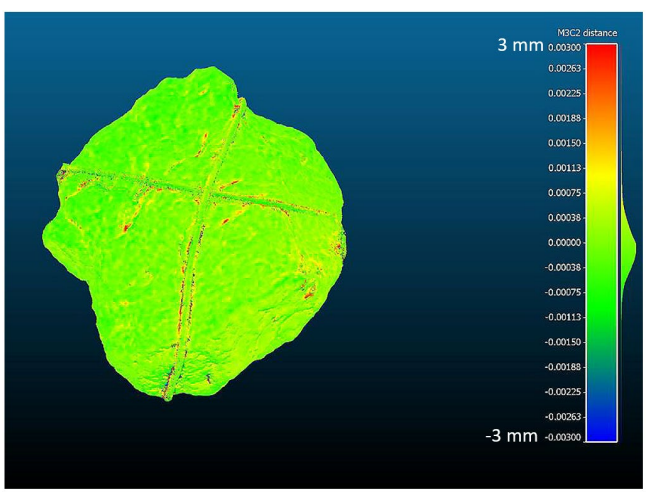

FIGURE 12. Comparison of dense point clouds using the M3C2 method in CloudCompare.

Figure 13 shows the difference between the point cloud obtained from the images taken with the camera and the point cloud generated with the images obtained with the UAS. After reviewing the point cloud resulting from the comparison, an interval of between -0.003 and 0.003 meters was established for its representation, as the points corresponding to greater distances were disregarded since they form part of the region of the specimen test where the ropes are placed and are of no interest for the study. Figure 14 shows a histogram which demonstrates that 87.45% of the points are in the distance range between -1 and +1 mm. This implies that the results obtained with the UAS camera and the DSLR camera show a residual discrepancy.

3D COMPARISON OF DISTANCE MEASUREMENT

The second method of validating the results consisted of comparing the measurement of distances on the model and on multiple points on the test specimen. As indicated above, a total of 26 singular points on the object were selected which, grouped in pairs, resulted in 13 distances. The points of interest were selected on all faces of the test specimen. The distances in the model were measured using Metashape™. To do this, the 26 selected points in the images were located using markers. Once located, the "Create Distance Measurement" tool was used to measure the distance between each pair of points. Table 5 shows the results of the measurements taken on the model and the object, the relative error in % and the absolute error in mm. The mean relative error is 1.49%, the mean absolute error is 1.1 mm. In the two right-hand columns the mean statistical error of 0.16 mm and a standard deviation of 1.42, which show the low dispersion of the data are also presented. The graph in Figure 16 was composed from this table. Although the values in the table already shown an extremely low level of error, in order to verify the results more precisely, some basic statistical calculations were made with the data from the table and the graph referred to above. Figure 14 shows on the ordinate axis the dimensional values obtained in the model and on the abscissa axis those measured on the object. The red dotted line corresponds to the linear regression of the data series. The labels show the values from table 4. The practically linear fit of the measurements shows an almost perfect correlation between the two data series. Although the results were predictable, since the manual measurements and those obtained from the model have a certain level of random error, Pearson's correlation coefficient was calculated, [35]. The correlation coefficient of two variables is a measure of their linear dependence. The correlation result was 0.9994, in real terms 1, indicating a perfect fit. In order to present the experimental procedure and the difficulty of manual measurement, a mosaic of photographs of some of the measurements is shown in Figure 15. The points selected this figure are singularities of the rock which can be seen with the naked eye and can be found on any other object subjected to the same procedure. Their location on the model for checking purposes is therefore easy and straightforward. It is important to note that the granular nature of granite rock and its continuous manipulation makes it susceptible to material loss during the positioning of the caliper tips. Furthermore, although the points for measurement were chosen because they were easily identifiable to the naked eye, it was found that even in successive measurements at the same point there was a random error that is added to or subtracted (it is random in nature) from the 0.01 mm resolution of the tool.

FIGURE 13. **Histogram of the point cloud generated using M3C2.**

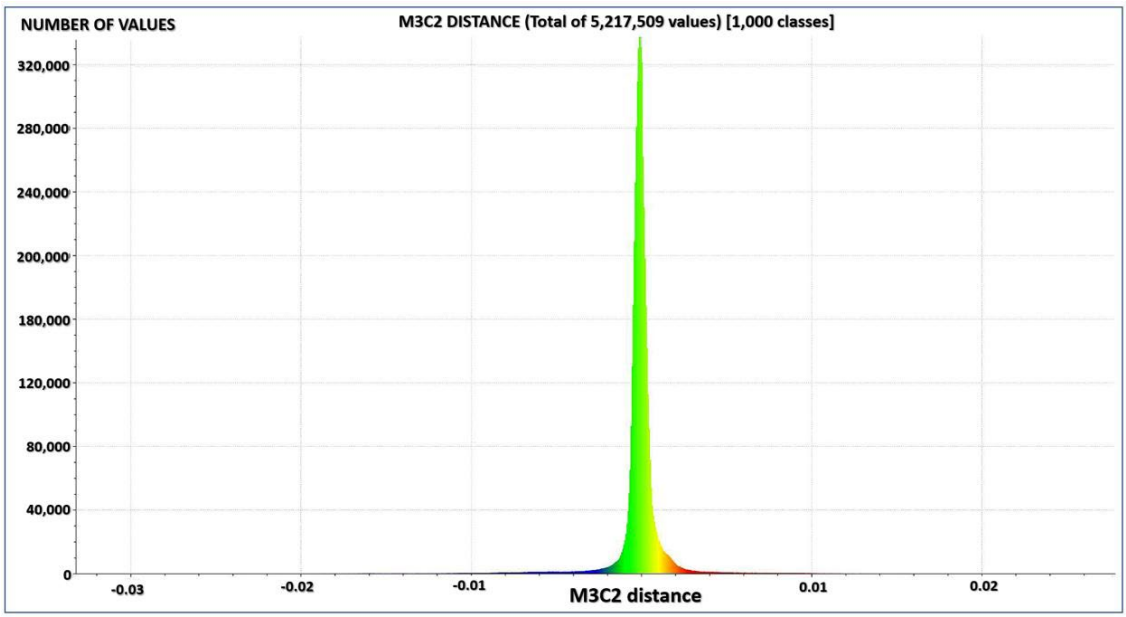

TABLE 6: 3D model data and error measurement

MODEL DISTANCE (mm)	OBJECT DISTANCE (mm)	RELATIVE ERROR %	ABSOLUTE ERROR (mm)	ERROR (mm)	ERROR MEAN	ERROR STD. DEVIATION
33.48	32.78	2.09	0.7	0.7	0.16	1.42
36.62	38.46	5.02	1.84	-1.84		
49.25	49.14	0,22	0.11	0.11		
62.24	62.99	1.21	0.75	-0.75		
66.46	67.68	1.84	1.22	-1.22		
73.87	72.92	1.29	0.95	0.95		
87.98	87.47	0.58	0.51	0.51		
92.75	92.35	0.43	0.4	0.4		
109.04	111.4	2.16	2.36	-2.36		
111.29	108.55	2.46	2.74	2.74		
131.6	129.68	1.46	1.92	1.92		
146.19	145.34	0.58	0.85	0.85		
147.52	147.45	0.05	0.07	0.07		

In spite of all these limitations, the final result, to be shown later, demonstrates that this new method produces models with a high-quality dimensional fit, which allows the authors to affirm that its application does not imply the use of complex distance measuring instruments nor, of course, GCPs. A graph showing the error of the measurements and their average value will be presented in Figure 14. The random variability of the error can be observed; in some measurements the error it is practically nil, while in others rational discrepancies are found. Despite these variations, the mean relative error is exceptionally low for an analysis of these characteristics. It presents a value of 1.49%. The mean value of the absolute error is 1.1 mm, in line with the previous one, and valid for the three-dimensional reconstruction of the test specimen or any other object. In a later section, two aspects not covered so far will be discussed; the influence of the size of the test specimen and the use of the scaling tool and the method developed outdoors.

The final result is the 3D model. Figure 17 shows it from different angles. In order to allow a better observation from all perspectives and to assess the quality of the result, it has been published on the Sketchfab Platform. It can be viewed at the following link: Interactive 3D model.

FIGURE 14. **Object measurements vs. model measurement and linear regression for the data series.**

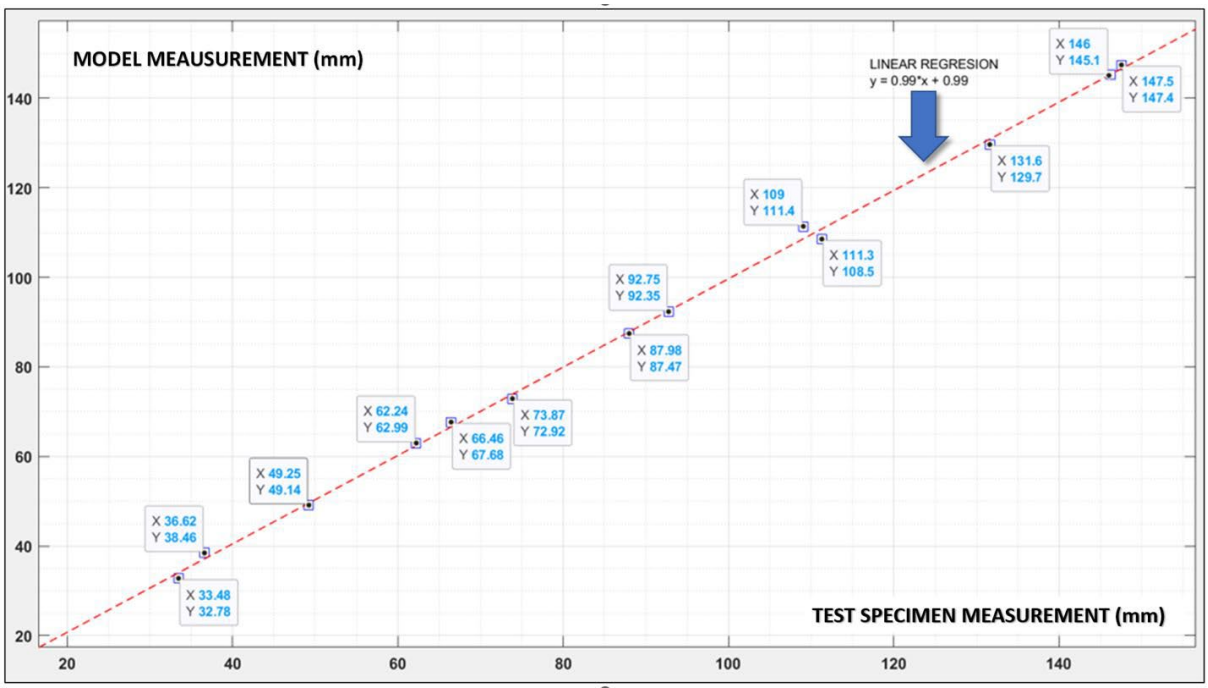

Although it is not the objective of this research, it is important to point out that the work carried out opens up possibilities for use in geotechnical studies. In particular, for the characterization of Rock Joint Micro-Scale Surface Roughness and Rock Discontinuity Roughness, [36], [37]. These studies could be approached in two different ways. As many areas as desired could be sampled by deploying as many target systems as desired. By having a GPS signal, the coordinates where they have been released would be known and could be retrieved in the same way as they were removed from the test specimen in this study. A second possibility [37] for large-scale sampling would be to deploy GCPs from the UAS, which would simplify the process and avoid the need for a technician to travel to do it manually [37]

C. SIZE OF THE TEST SPECIMEN

Since the investigation has been carried out on a relatively small test specimen, it might be questioned whether the procedure is valid on larger objects or not, and indeed it is. The scaling tool is light but solid as the prism walls are 3 mm thick. Whether 3D printed or built on paper, as mentioned in previous sections, its dimensions can be increased without weight being a problem. For example, a scaled 1:4 ratio tool, built with printed paper, would yield to a maximum weight of 16 gr, which is ¼ of the weight of the 3D printed tool and, therefore valid for the Mavic Mini 1 and negligible for any other UAS of the same series, capable of carrying up to 500 grams. The only possible drawback would be the oscillations that could be caused by the vortexes of the propellers. This could be solved by modifying the fastening and deployment system. If the size of the UAS is increased, the presumed aerodynamic interference is obviously significantly reduced. Should the dimensions of the test specimen require it, two scaling tools with larger photogrammetric targets could be deployed on the object. After the presentation and verification of the new 3D modelling method, in order to show that in real cases the conditions for the deployment of the scaling tool are re-ally simple, the Figure 18 shows a future work of the authors: the 3D and dimensionally accurate reconstruction of the capitals of the figure, where the surface on which the prism will be deployed is marked with arrows.

A. CONCLUSIONS

A new procedure, based on the present SfM-VMs techniques and software, has been developed, to the best of the authors' knowledge, which makes it possible to obtain 3D scale models indoors, in the absence of GPS positioning, and more importantly for objects where access is very complex or involves the installation of additional infrastructure. Only a Low-Cost UAS, a scaling tool and a caliper have been used.

The accuracy of the 3D modelling has been validated by comparing the point clouds generated from the set of photos taken manually with a DSLR camera, and those collected by the UAS camera. The result of the comparison shows that the existing differences are negligible.

The complexity and cost ratio with respect to the quality of the result obtained is high. It has been shown that the average absolute error of the model, with respect to the test specimen, including the random error of the manual measurement, is 1.47% in relative terms 1.1 mm, the mean error is 0.16 mm and its standard deviation 1.42. Although the error may seem

non-negligible and is obviously larger than that which would be obtained high-resolution scanners, it is important to bear in mind two aspects: on the one hand, the error presented has been established from a set of manual measurements, made with a caliper, on a material of a granular nature. It is therefore impossible to take the tolerance of the caliper as a reference to determine the possible random error of the direct measurements.

On the other hand, the use of the aforementioned high-precision instrumentation implies a very high cost and a more complex handling that puts it beyond the reach of many users and/or researchers.

This article shows the validity of the developed method although it is necessary to carry out field studies and validations, on objects, as well as using a high-resolution scanner, which would replace the DSLR camera to determine with unquestionable precision the level of error in the comparison of the point clouds. The ease of handling of the UAS when transporting the scaling tool, and the simplicity of its placement and subsequent collection has been verified and documented under more adverse conditions than those of field-study case [34]. A comparison of the area for the placement of the scaling tool, as shown in Figure 18, a large, flat, uncluttered surface, compared to the conditions shown in [34], where space is minimal, lighting is low and all UAS positioning and navigation aids were deliberately disabled, demonstrates that its application in real cases is feasible and simple

B. ACKNOWLEDGEMENT

This study has been funded by the Xunta de Galicia, through the grants for the consolidation and structuring of competitive research units in the universities of the Galician University System (2020-2022) Ref. ED341D R2016/023. In turn, thanks are due to the Ministry of Education and Vocational Training (collaboration grants 2020-2021) and to the new structure derived from the transformation of the BioReDes Strategic Grouping (grants 2021). Finally, the authors would like to thank Marcos Arza García, researcher of the CIGEO group at the University of Santiago de Compostela, for his assistance and guidance during the development of the research.

FIGURE 15. **Some of the manual measurements carried out on singular points of the test specimen.**

FIGURE 16. **Relative error (%) vs. measured distance and mean relative error.**

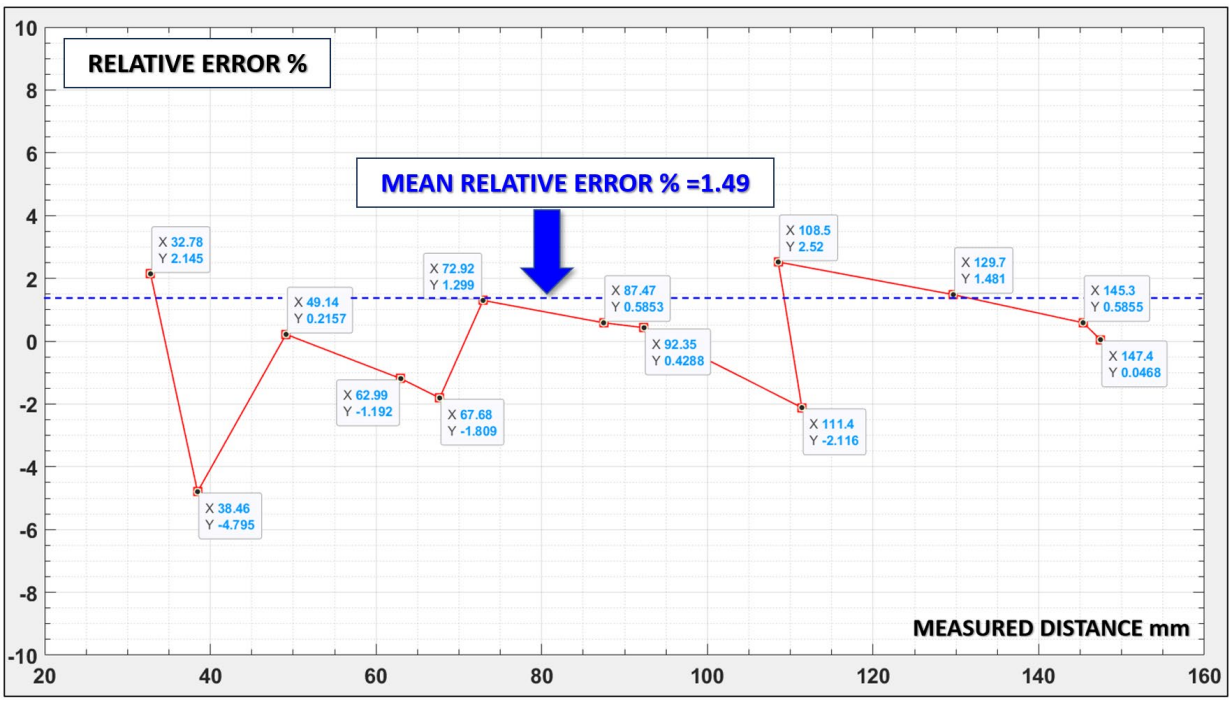

FIGURE 17. **3D model generated in Agisoft Metashape from the images obtained the UAS.**

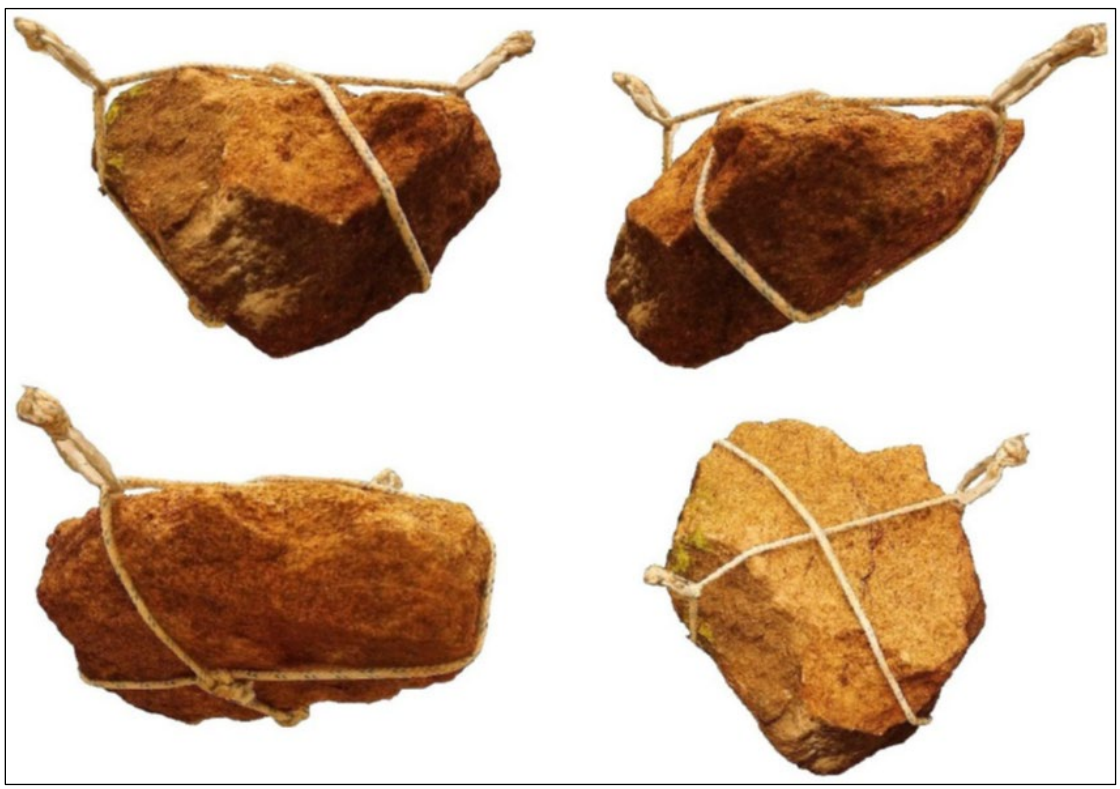

FIGURE 18. **Future study of the authors.**

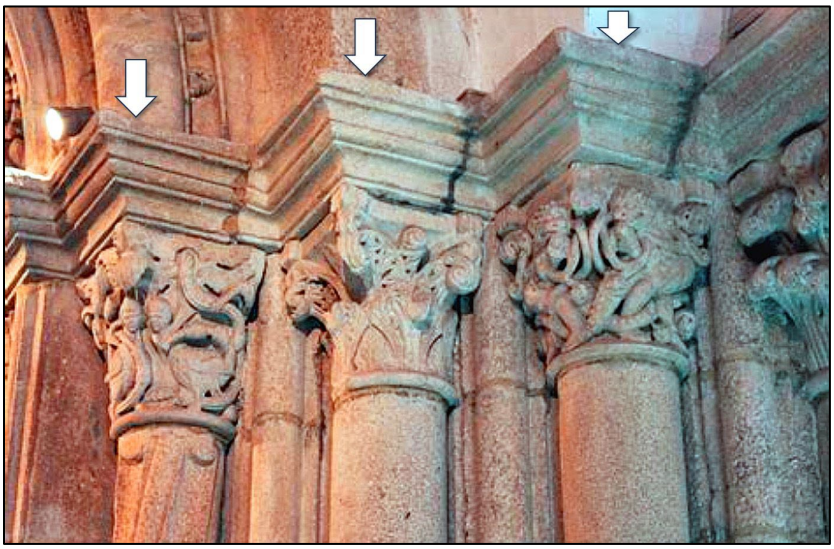

REFERENCES

[1]. Shakhatreh, H., Sawalmeh, A. H., Al-Fuqaha, A., Dou, Z., Almaita, E., Khalil, I., Othman, N. S., Khreishah, A., Guizani, M. (2019). Unmanned Aerial Vehicles (UAVs): A Survey on Civil Applications and Key Research Challenges. IEEE Access, 7: 48572–48634, DOI: https://dx.doi.org/10.1109/ACCESS.2019.2909530.

[2]. Adami, A., Fregonese, L., Gallo, M., Helder, J., Pepe, M., Treccani, D. (2019). Ultra-Light UAV Systems for the Metrical Docu-mentation of Cultural Heritage: Applications for Architecture and Archaeology. The International Archives of the Photogrammetry, Remote Sensing and Spatial Information Sciences, XLII-2/W17: 15–21, DOI: https://dx.doi.org/10.5194/isprs-archives-XLII-2-W17-15-2019

[3]. Hashim, K. A., Ahmad, A., Samad, A. M., NizamTahar, K., Udin, W. S. (2012). Integration of low altitude aerial & terrestrial photogrammetry data in 3D heritage building modeling. 2012 IEEE Control and System Graduate Research Colloquium, 225–230, DOI: https://dx.doi.org/10.1109/ICSGRC.2012.6287166

[4]. Zollini, S., Alicandro, M., Dominici, D., Quaresima, R., Giallonardo, M. (2020). UAV Photogrammetry for Concrete Bridge In-spection Using Object-Based Image Analysis (OBIA). Remote Sensing, 12(19): 3180, DOI: https://dx.doi.org/10.3390/rs12193180

[5]. Germanese, D., Leone, G., Moroni, D., Pascali, M., Tampucci, M. (2018). Long-Term Monitoring of Crack Patterns in Historic Structures Using UAVs and Planar Markers: A Preliminary Study. Journal of Imaging, 4(8): 99, DOI: https://dx.doi.org/10.3390/jimaging4080099

[6]. Kalaitzakis, M., Kattil, S. R., Vitzilaios, N., Rizos, D., Sutton, M. (2019). Dynamic Structural Health Monitoring using a DIC-enabled drone. 2019 International Conference on Unmanned Aircraft Systems (ICUAS), 321–327, DOI: https://dx.doi.org/10.1109/ICUAS.2019.8798270

[7]. Roca, D., Lagüela, S., Díaz-Vilariño, L., Armesto, J., Arias, P. (2013). Low-cost aerial unit for outdoor inspection of building façades. Automation in Construction, 36: 128–135,

DOI: https://dx.doi.org/10.1016/j.autcon.2013.08.020

[8]. Larrinaga, A., Brotons, L. (2019). Greenness Indices from a Low-Cost UAV Imagery as Tools for Monitoring Post-Fire Forest Recovery. Drones, 3(1): 6, DOI: https://dx.doi.org/10.3390/drones3010006

[9]. Lagüela, S., Díaz−Vilariño, L., Roca, D., Lorenzo, H. (2015). Aerial thermography from low-cost UAV for the generation of thermographic digital terrain models. Opto-Electronics Review, 23(1): 76–82, DOI: https://dx.doi.org/10.1515/oere-2015-0006

[10] Oniga, E., Chirilă, C., Stătescu, F. (2017). Accuracy Assessment of a 3D Model Reconstructed from Images Acquired with a Low-Cost UAV. The International Archives of the Photogrammetry, Remote Sensing and Spatial Information Sciences, XLII-2/W3: 551–558, DOI: https://dx.doi.org/10.5194/isprs-archives-XLII-2-W3-551-2017

[11]. Benkhoui, Y., El Korchi, T., Reinhold, L. (2019). UAS-Based Crack Detection Using Stereo Cameras: a Comparative Study. 2019 International Conference on Unmanned Aircraft Systems (ICUAS), 1031–1035, DOI: https://dx.doi.org/10.1109/ICUAS.2019.8798311

[12]. Balaguer Puig, M. (2017). Fotogrametría de Objeto Cercano: Conceptos básicos. http://hdl.handle.net/10251/82148

[13]. Jiang, R., Jáuregui, D. V., White, K. R. (2008). Close-range photogrammetry applications in bridge measurement: Literature review. Measurement, 41(8): 823–834, DOI: https://dx.doi.org/10.1016/j.measurement.2007.12.005

[14]. Tomás, R., Riquelme, A., Cano, M., Abellán, A. (2016, octubre). Structure from Motion (SfM): una técnica fotogramétrica de bajo coste para la caracterización y monitoreo de macizos rocosos. En 10º Simposio Nacional de Ingeniería Geotécnica (pp. 209-2016). A Coruña.https://www.researchgate.net/publication/309611177_Structure_from_Motion_SfM_una_tecnica_fotogrametrica_de_bajo_coste_para_la_caracterizacion_y_monitoreo_de_macizos_rocosos

[15]. Gonçalves, G., Gonçalves, D., Gómez-Gutiérrez, Á., Andriolo, U., Pérez-Alvárez, J. A. (2021). 3D Reconstruction of Coastal Cliffs from Fixed-Wing and Multi-Rotor UAS: Impact of SfM-MVS Processing Parameters, Image Redundancy and Acquisition Geometry. Remote Sensing, 13(6): 1222, DOI: https://dx.doi.org/10.3390/rs13061222

[16]. Narciso, E. M., García, J. H., Pérez-Alberti, A. (2016, 22-25 de junio). Estudio de la dinámica geomorfológica mediante la ob-tención de modelos topográficos históricos y actuales a partir de fotogrametría digital automatizada: acantilados de A Capelada (A Coruña, Galicia). En XIV Reunión de la Sociedad Española de Geomorfología. Málaga. https://www.researchgate.net/publication/308011087

[17]. Souto-Vidal, M., Ortiz-Sanz, J., Gil-Docampo, M. (2015). Implementación del levantamiento eficiente de fachadas mediante fotogrametría digital automatizada y el uso de software gratuito. Informes de La Construcción, 67(539): e107, DOI: https://dx.doi.org/10.3989/ic.14.098

[18]. Gil-Docampo, M., Peña-Villasenín, S., Ortiz-Sanz, J. (2020). An accessible, agile and low-cost workflow for 3D virtual analysis and automatic vector tracing of engravings: Atlantic rock art analysis. Archaeological Prospection, 27(2): 153–168, DOI: https://dx.doi.org/10.1002/arp.1760

[19]. Aicardi, I., Chiabrando, F., Grasso, N., Lingua, A. M., Noardo, F., Spanò, A. (2016). UAV Photogrammetry with Oblique Images: First Analysis on Data Acquisition and Processing. The International Archives of the Photogrammetry, Remote Sensing and Spatial Information Sciences,

XLI-B1: 835–842, DOI: https://dx.doi.org/10.5194/isprsarchives-XLI-B1-835-2016

[20]. Grottoli, E., Biausque, M., Rogers, D., Jackson, D. W. T., Cooper, J. A. G. (2020). Structure-from-Motion-Derived Digital Surface Models from Historical Aerial Photographs: A New 3D Application for Coastal Dune Monitoring. Remote Sensing, 13(1): 95, DOI: https://dx.doi.org/10.3390/rs13010095

[21]. Lastilla, L., Belloni, V., Ravanelli, R., Crespi, M. (2021). DSM Generation from Single and Cross-Sensor Multi-View Satellite Images Using the New Agisoft Metashape: The Case Studies of Trento and Matera (Italy). Remote Sensing, 13(4): 593, DOI: https://dx.doi.org/10.3390/rs13040593

[22]. Peña-Villasenín, S., Gil-Docampo, M., Ortiz-Sanz, J. (2020). Desktop vs. cloud computing software for 3D measurement of building façades: The monastery of San Martín Pinario. Measurement, 149: 106984, DOI: https://dx.doi.org/10.1016/j.measurement.2019.106984

[23]. Armesto, J., Arias, P., Roca, J., Lorenzo, H. (2008). Monitoring and Assessing Structural Damage in Historic Buildings. The Photogrammetric Record, 23(121): 36–50, DOI: https://dx.doi.org/10.1111/j.1477-9730.2008.00466.x

[24]. Khosiawan, Y., Nielsen, I. (2016). A system of UAV application in indoor environment. Production and Manufacturing Research, 4(1): 2–22, DOI: https://dx.doi.org/10.1080/21693277.2016.1195304

[25]. Dowling, L., Poblete, T., Hook, I., Tang, H., Tan, Y., Glenn, W., Unnithan, R. R. (2018). Accurate indoor mapping using an autonomous unmanned aerial vehicle (UAV). ArXiv, https://arxiv.org/abs/1808.01940

[26]. Mining Drones: ELIOS 2 Creates Photogrammetric Models of a Gold Mine Previously Impossible to Inspect. (2019). Short URL (rb.gy/zbntbp), please, copy and paste de text.

[27]. Kerle, N., Nex, F., Gerke, M., Duarte, D., Vetrivel, A. (2019). UAV-based structural damage mapping: A review. ISPRS Inter-national Journal of Geo-Information, 9(1): 14, DOI: https://dx.doi.org/10.3390/ijgi9010014

[28]. Nikolic, J., Burri, M., Rehder, J., Leutenegger, S., Huerzeler, C., Roughness Characterisation usingPhotogrammetry Method, Journal of Mining and Environment (JME), DOI: https://doi.org/10.22044/jme.2022.11669.2155

[37]. Riccardo Salvini, Claudio Vanneschi, John S. Coggan, Giovanni Mastrorocco, P. (2020). Evaluation of the Use of UAV Photo-grammetry for Rock Discontinuity Roughness Characterization, Rock Mechanics and Rock Engineering, DOI: https://doi.org/10.1007/s00603-020-02130-2

Siegwart, R. (2013, 2-9 de marzo). A UAV system for inspection of industrial facilities. En 2013 IEEE Aerospace Conference (pp. 1-8). Big Sky, MT, USA: IEEE.

DOI: https://dx.doi.org/10.1109/AERO.2013.6496959

[29]. Fort, R., Alvarez de Buergo, M., Perez-Monserrat, E. M. (2013). Non-destructive testing for the assessment of granite decay in heritage structures compared to quarry stone. International Journal of Rock Mechanics and Mining Sciences, 61 296–305, DOI: https://dx.doi.org/10.1016/j.ijrmms.2012.12.048

[30]. Pozo-Antonio, J. S., Rivas, T., López, A. J., Fiorucci, M. P., Ramil, A. (2016). Effectiveness of granite cleaning procedures in cultural heritage: A review. Science of The Total Environment, 571 1017–1028, DOI: https://dx.doi.org/10.1016/j.scitotenv.2016.07.090

[31]. Fernández Suárez, J., Álvarez Areces, E., Martín, J. M. B. (2016). Evolución histórico-geográfica de la extracción de piedra natural para la construcción civil y religiosa de San Ciprián (N de Lugo, Galicia). IX Congreso Geológico de España, 16(2): 375-378. https://sge.usal.es/archivos/GEO_TEMAS/Geo_temas16_ss_simposios.pdf

[32]. Martínez-Senra, A. I., Guisado-Tato, M. (2000). La industria del granito en Galicia. Boletín Económico de ICE, 2669, https://www.researchgate.net/publication/28120585

[33]. Aicardi, I., Angeli, S., Grasso, N., Lingua, A. M., Maschio, P. (2020). Geomatic Techniques for the optimization of ski resources. The International Archives of the Photogrammetry, Remote Sensing and Spatial Information Sciences, XLIII-B2-2020: 1009–1016, DOI: https://dx.doi.org/10.5194/isprs-archives-XLIII-B2-2020-1009-2020

[34]. Scaling tool deployment and flight demonstration https://youtu.be/4z19HH6eCbo

[35]. Press, W.H., Teukolsky, S.A., Vetterling, W.T., and Flannery, B.P. Numerical Recipes in C, 2nd Ed., Cambridge University Press, 199.

[36]. Mojtaba Bahaaddini, Mehdi Serati, Mohammad Hossein, Khosravi and Bruce Hebblewhite P. (2022), Rock Joint Micro-Scale Surface

FIRST A. AUTHOR. M. L. Gil-DOCAMPO

Was born in A Coruña, Spain, in 1968. She received the Ph.D. degree from the University of Santiago de Compostela, Spain, in 2001. In 1996, she joined the Department of Agroforestry Engineering, University of Santiago de Compostela, where she is currently an Associate Professor. Her main research interests are in the field of applications of Unmanned Aerial Systems (UAS). She is the head of the CIGEO group on this topic. She is also coordinating a master's degree in UAS and its applications.

SECOND B. AUTHOR. S. Peraleda-Vázquez

She was born in Lugo, Spain, in 1994. She received her B.S. degree in Agricultural Engineering from the University of Santiago de Compostela, Spain, in 2018, as well as her Master's degree in Operations and Unmanned Aircraft Systems Engineering in 2021. She is developing her Ph.D on the topic of UAS imagery applications. She is also working at the Engineering Insitu™ company in this field of study

THIRD C. AUTHOR. J. Ortiz Sanz

He received his B.S. degree in Agricultural Engineering from the University of Valladolid, Spain, in 1989, a M.S. degree in Agricultural engineering from the University of Santiago de Compostela, Spain, in 1993 and the Ph.D. degree in Agricultural Engineering from the University of Santiago de Compostela, Spain, in 2008. Since 1995, is a Professor with the Agroforestry Engineering Department, University of Santiago de Compostela. He is the author of three books and more than 20 articles. His main research interests include the use of close-range photogrammetry in recording cultural heritage, structural analysis, and rural building. He is a Researcher with the CIGEO (Civil & Geomatics) research group, and the main researcher of D3MOBILE project. Prof. Ortiz-Sanz was a recipient of the XIV 3M Foundation Award for innovation in 2012.

FOURTH D. AUTHOR. M. F. Cabanas

(M'97) was born in Gijón, Spain, in 1965. He received the Ph.D. degree from the University of Oviedo, Gijón, Spain, in 1995. In 1992, after working for two years in the Defense Sector (NATO) he joined the Department of Electrical Engineering, University of Oviedo, where he is currently an Associate Professor. His main research interests are in the field of diagnostics of electrical and Unmanned Aerial Systems (UAS). He is the head of two research groups on both areas respectively: He is the author of a book, 40 papers in journals and more than 100 conferences and congress communitations.

ANEX I: TARGETS